Research Article

International Journal of
Protective Structures

International Journal of Protective Structures
2016, Vol. 7(1) 18–44

DOI: 10.1177/2041419615622726
prs.sagepub.com
SAGE

Duality of energy absorption and inertial effects: Optimized structural design for blast loading

Marcus P Rutner[1] and Joseph P Wright[2]

Abstract

This article provides insights into the dynamic response and protection capacity of sacrificial structures mounted on a structural member and subjected to close standoff blast loading. The three main objectives of this study are: (a) exploration of key parameters governing the failure modes of a structural member protected by a sacrificial structure; (b) quantification of blast resistance and protection capacity of the sacrificial structure and underlying structure; and (c) conducting comparative single-degree-of-freedom system analysis and high-resolution explicit finite element analysis aiming at improving current single-degree-of-freedom analysis approaches. Energy absorption and momentum resistance are identified and quantified as the main contributing mechanisms controlling the dynamic response of structural members subjected to high-speed dynamic loading. The displacement of the structural member in the blast direction, the mass per length of the structural member, and the maximum impulse are found to be parameters governing the nonlinear response. The article also presents a response surface approach which might have value for time-efficient optimized structural member design and prediction of nonlinear structural member response to blast loading. This study includes validation of the numerical data through free-air blast test data from the literature.

Keywords

Sacrificial structure, single-degree-of-freedom, finite element analysis, load–mass factor, blast loading

Introduction

The authors Xue and Hutchinson (2003), Hutchinson and Xue (2005), Vaziri et al. (2007), and Vaziri et al. (2006) investigated the blast performance of all-metal sandwich plates in comparison with a solid metal plate of the same mass. Several sandwich core types were studied, including rectangular honeycomb cells (Hutchinson and Xue, 2005), the folded sandwich plate

[1]Department of Civil, Environmental and Ocean Engineering, Stevens Institute of Technology, Hoboken, NJ, USA
[2]Weidlinger Associates, Inc., New York, NY, USA

Corresponding author:
Marcus P Rutner, Department of Civil, Environmental and Ocean Engineering, Stevens Institute of Technology, 1 Castle Point on Hudson, Hoboken, NJ 07030-5991, USA.
Email: marcus.rutner@stevens.edu

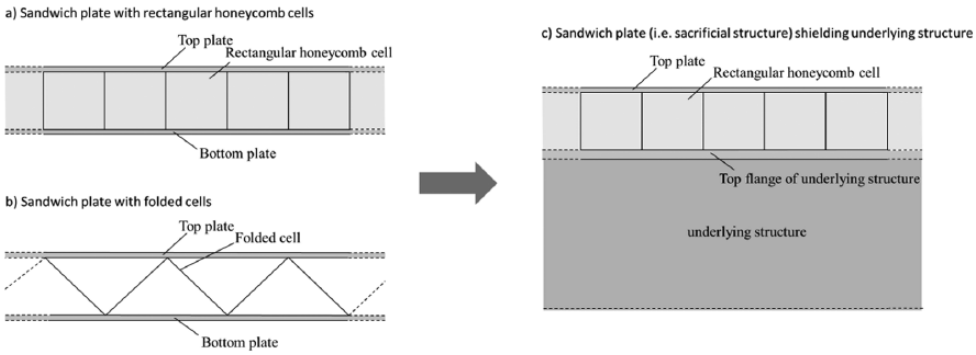

Figure 1. (a) Metal sandwich plate configurations with square honeycomb cells and (b) folded cell structure; (c) sacrificial structure mounted on an underlying structure, that is, the structure to be protected.

cell structure (Vaziri et al., 2007), the tetragonal truss core structure (Xue and Hutchinson, 2003), as well as the rectangular honeycomb structure filled with polymer foam (Vaziri et al., 2006). The square honeycomb sandwich plate and the folded sandwich plate are shown in Figures 1(a) and (b).

Rectangular honeycomb cells provide high crushing strength and energy absorption (Hutchinson and Xue, 2005). The identified failure modes of an all-metal sandwich plate are shearing off the front face plate and bending of the total plate which, at larger loads, transforms into catenary action (Hutchinson and Xue, 2005) with hinges at the bearings as well as along the plate center. Superior performance was attributed to all-metal sandwich plates in comparison with solid plates of same mass subjected to air-blast pressure. An approximate analytical approach (Fleck and Deshpande, 2004), which characterizes the dynamic plate response and distinguishes three stages: the fluid–structure interaction (stage 1); the core crushing (stage 2); and the overall bending and stretching (stage 3), is adopted by Hutchinson and Xue (2005). The blast load is idealized as a short duration pulse loading the front face of the sandwich plate with uniform pressure (Hutchinson and Xue, 2005; Vaziri et al., 2007; Xue and Hutchinson, 2003).

In Hutchinson and Xue (2005), the authors introduced μ as a measure of relative mass of the sandwich element core, $\mu = m_c / m_f$, where m_c and m_f are the mass of the all-metal sandwich core and the front plate, respectively. It is emphasized that the analysis approach introduced in Hutchinson and Xue (2005) only considers a relatively low impulsive blast loading that does not cause full densification of the sandwich plate.

The all-metal rectangular honeycomb cell structure as investigated in Xue and Hutchinson (2003), Hutchinson and Xue (2005), and Vaziri et al. (2007) is adopted herein as a sacrificial cell structure mounted on an underlying structure, as illustrated in Figure 1(c), which defines a *new system* with new boundary conditions. The dynamic response of this system is investigated accounting for full densification of the honeycomb cells. The densification process is defined in Gibson and Ashby (1997). The objectives of this study are as follows:

- To define the key design parameters governing the failure mode of the underlying structure which is shielded by a sacrificial structure subjected to blast loading. One interesting question which arises is whether the relative mass μ, as introduced in Hutchinson and Xue (2005),

also plays an important role in protecting an underlying structure, that is, structural members, shielded by sacrificial metal honeycombs. In this study, analytical methods, that is, single- and two-degree-of-freedom (SDOF/2DOF) systems, and high-fidelity explicit finite element (FE) analysis (Vaughan, 1983) are used. Validation of the numerical analysis is also included.

- To understand and quantify the protection capacity of a lightweight honeycomb sacrificial cell structure mounted on an underlying structure when subjected to blast loading. Various protection measures are investigated and ranked by effectiveness.
- To critically prove whether high-resolution FE analysis results can be used to improve equivalent SDOF/2DOF system analysis.

These objectives add to findings made by Starr and Krauthammer (2005), which reveal that the impact force dissipation through sacrificial cladding is about 25–50% depending on loading conditions, without specifying whether the force dissipation happened through energy absorption or momentum resistance.

The authors Fujikura et al. (2008) pointed out the research need for high-resolution FE models to better understand the behavior of complex structural systems and to conduct parametric studies; they investigated reinforced columns and also evinced interest in studies of steel-jacketed columns exposed to blasts. Our article will focus on air- and concrete-filled steel columns subjected to close-in blast loading.

A summary of SDOF modeling of structural members subjected to lateral blast loading is given in Cormie et al. (2009). Various analytical methods are described in Winget et al. (2005) comparing their strengths and weaknesses. The maximum displacement of such members is given in equation (1)

$$X_M = \frac{1}{2}\left(\frac{I^2}{K_{LM} m r_u} + X_E \right) \tag{1}$$

where X_M and X_E are maximum and elastic deflection, and I, K_{LM}, m, and r_u are reflected impulse, load–mass factor, mass, and ultimate resistance of the column per unit length, respectively. The load–mass factor K_{LM} is the ratio of mass factor K_M and load factor K_L. The equations for K_M and K_L are shown in equations (2) and (3)

$$K_M = \frac{\int_0^L m\phi^2(x)\,\mathrm{d}x}{mL} \tag{2}$$

$$K_L = \frac{\int_0^L p(x)\phi(x)\,\mathrm{d}x}{pL} \tag{3}$$

While mass m and resistance r_u can be determined explicitly, since they depend only on density, cross-sectional design, and boundary conditions, respectively, the load–mass factor depending on load distribution and deflection along the beam is unknown (Biggs, 1964). The load–mass factor for the plastic response of a simple girder is 0.33 for a centric single load, but becomes 0.66 for a uniform load (Cormie et al., 2009; Fujikura and Bruneau, 2012). This article will provide further insights as to reasonable values of K_{LM} for small-standoff explosive threat.

The maximum displacement is defined in terms of maximum rotation angles or maximum ductility (Cormie et al., 2009). Using the results of FE analysis, the adequacy of these deformation limits is discussed in this article.

Sacrificial structure and underlying structure

The underlying structure is a column consisting of an AISC W14 × 233 section with 2.72-cm-thick steel side plates, constituting a typical design for a perimeter ground floor column of a 20-story building. The column height is 5.48 m. The column is installed in a moment frame structure using AISC W24 × 55 beams, as shown in Figure 2(a). The horizontal moment frame is rigidly fixed in the symmetry plane opposite the column. The column member is rigidly fixed at ground level and symmetry boundary conditions are applied along the edges of the reinforced concrete slab. The column top is loaded vertically by the gravity load of 12.45 MN which corresponds to the axial loading of a ground floor column in a 20-story building. Three different blast charge sizes, measured in terms of maximum reflected impulse sensed on the column target surface in the symmetry plane and at charge level, are investigated, that is, 0.049, 0.091, and 0.133 MPa s. The blast load level causing a maximum reflected impulse of 0.091 MPa s deforms but not fully densifies the metal sacrificial cells; the third blast level (0.133 MPa s) causes full densification of the sacrificial cell structure. The structure as idealized in the FE model and the charge location is shown in Figure 2(b). The center of the charge is located about 1.22 m above ground level. The blast loading is generated through computational fluid dynamics modeling (Wardlaw et al., 2003) and further compared using Hyde (1992) and Kingery and Bulmash (1984). The column and the horizontal frame structure supporting the column top are loaded by the blast pressure.

The material constitutive models representing the nonlinear behavior of the materials used in this study, that is, normal concrete, foam concrete, structural steel, and reinforcement steel, are available in the literature and extensively validated by experimental testing. For normal concrete, the rate-dependent three invariant softening model (Mould and Levine, 1994) is applied. The constitutive law for foam concrete is based on the nonlinear response of foam concrete as reported in Ehrgott (1973). The dynamic behavior of foam concrete is described by a cap model accounting for density which is primarily governing the high-speed dynamic loading response. The structural steel and reinforcement steel constitutive models are empirical material laws taking strain rate dependency, strain hardening, and softening of metals into consideration. All above constitutive laws are embedded in the material library of the explicit FE code applied in this study (Vaughan, 1983). Basic properties of the materials applied in this study are given in Table 1.

Structural hardening measures have been undertaken to ensure that the structural system connecting to the column top does not fail prior to column failure. Specifically, the beam supporting the column top in the blast direction is an AISC W24 × 55 beam encased in 27.58 MPa concrete.

Within an extensive computational study, in summary 30 cases of the structure-varying column design and load intensity have been investigated. The 30 cases are listed in Table 2. Column 1 of Table 2 gives the case number; columns 5 and 6 give information about the infill material of the sacrificial structure and the column core, respectively; columns 4 and 3 provide information about the total mass per length of the column and the maximum reflected impulse, respectively; and column 2 lists the permanent lateral displacement of the column in blast direction measured at charge level. Whenever displacement is mentioned in the following, it is referred to as the post-blast permanent lateral displacement measured at charge level.

The dynamic behavior of the sandwich plate mounted on the underlying structure is explored for three impulse levels, as specified above:

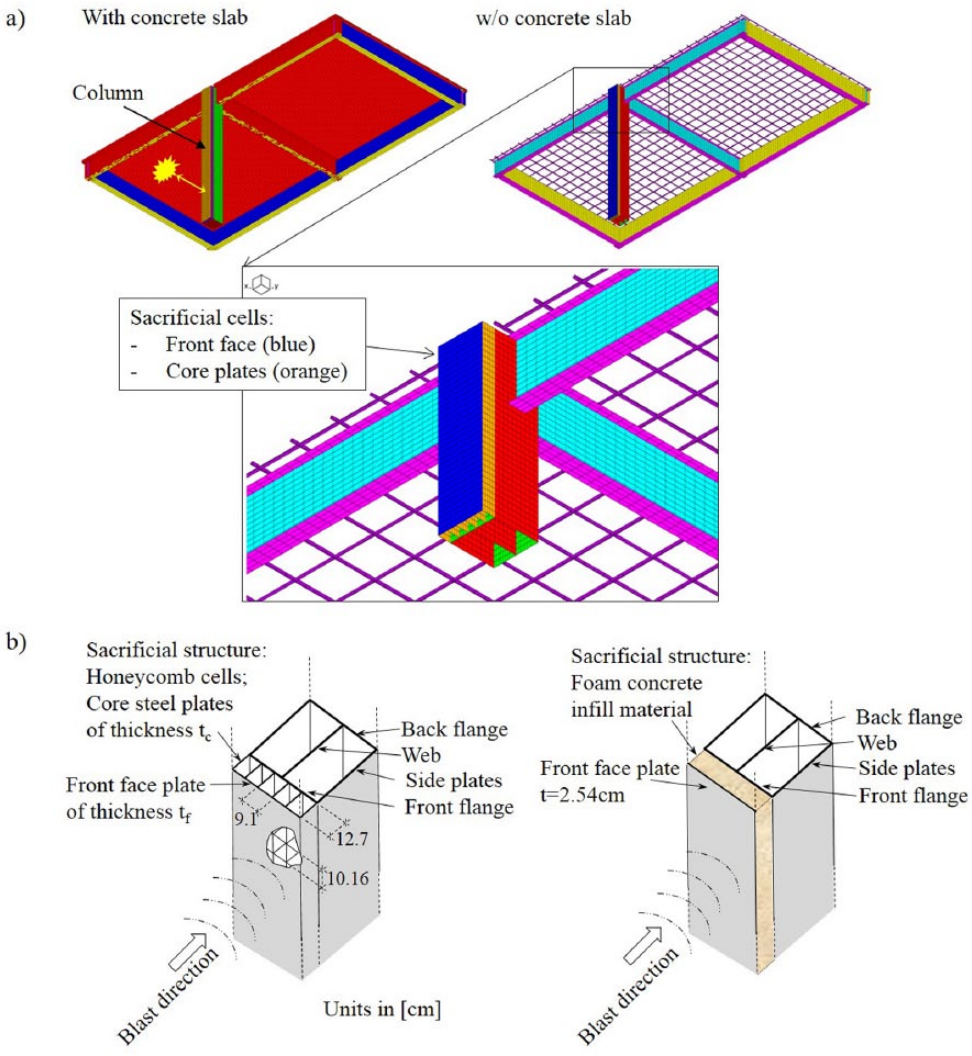

Figure 2. (a) Finite element model of the column, that is, the underlying structure shielded by all-metal honeycomb sacrificial cells, and (b) all-metal honeycomb sacrificial cells and foam concrete sacrificial layer mounted on underlying structure, that is, the air-filled column core section.

Table 1. Material properties.

Material	Young's modulus (MPa)	Poisson's ratio	Yield strength (MPa)	Density (kg/m^3)	Plateau stress (MPa)
Structural steel	200,000	0.3	345	7795	–
Normal concrete	28,000	0.2	27.58	2322	–
Foam concrete	20,000	0.2	25.00	1161.34	5.52

Table 2. A total of 30 different cases of varying column design and load intensity.

Case	Displacement (cm)	Max. refl. impulse (MPa s)	Total mass (kg/m)	Sacrificial structure	Column core
1	1.7	0.049	945.92	Air-filled/Design 3	Concrete-filled
2	2.69	0.049	938.28	Foam concrete	Concrete-filled
3	1.22	0.049	1251.56	Solid steel	Concrete-filled
4	3.3	0.049	749.81	Air-filled/Design 3	Air-filled
5	5.33	0.049	742.17	Foam concrete	Air-filled
6	2.03	0.049	1055.45	Solid steel	Air-filled
7	12.95	0.091	707.70	Air-filled/Design 1	Air-filled
8	12.44	0.091	727.51	Air-filled/Design 2	Air-filled
9	12.44	0.091	749.81	Air-filled/Design 3	Air-filled
10	5.99	0.091	945.92	Air-filled/Design 3	Concrete-filled
11	8.76	0.091	938.28	Foam concrete	Concrete-filled
12	3.86	0.091	1251.56	Solid steel	Concrete-filled
13	11.94	0.091	749.81	Air-filled/Design 3	Air-filled
14	15.75	0.091	742.17	Foam concrete	Air-filled
15	7.62	0.091	1055.45	Solid steel	Air-filled
16	18.16	0.091	616.20	–	Air-filled
17	13.51	0.091	756.28	–	Foam concrete
18	7.65	0.091	812.31	–	Concrete-filled
19	12.4	0.091	749.81	Air-filled/Design 3	Air-filled
20	9.53	0.091	889.89	Air-filled/Design 3	Foam concrete
21	5.99	0.091	945.92	Air-filled/Design 3	Concrete-filled
22	25.4	0.133	707.70	Air-filled/Design 1	Air-filled
23	26.2	0.133	727.51	Air-filled/Design 2	Air-filled
24	26.2	0.133	749.81	Air-filled/Design 3	Air-filled
25	13.13	0.133	945.92	Air-filled/Design 3	Concrete-filled
26	15.65	0.133	938.28	Foam concrete	Concrete-filled
27	7.92	0.133	1251.56	Solid steel	Concrete-filled
28	26.16	0.133	749.81	Air-filled/design 3	Air-filled
29	33.53	0.133	742.17	Foam concrete	Air-filled
30	14.73	0.133	1055.45	Solid steel	Air-filled

- Elastic response of sacrificial cells and underlying structure (Impulse Level 1);
- Partial densification of the sacrificial cells (Impulse Level 2);
- Full densification (compaction) of the sacrificial cells (Impulse Level 3).

Establishing an energy approach and comparing the change of kinetic energy through Impulse Levels 1–3 help to find the major parameters governing the impulsive response, and subsequently to better understand the physics in transient dynamics.

The undeformed system can be represented as a 2DOF system, as shown in Figure 3. The charge is placed at distance L_1 away from the boundary, as shown in Figure 3(a). The equivalent 2DOF system is shown in Figure 3(b). The underlying structure, that is, the column, is represented by mass M, while the sacrificial structure is represented by mass m. Springs indicate elasto-plastic resistance functions that connect the masses to each other and to the ground. The nonlinear resistance function r represents the stiffness of the sacrificial structure, and R represents the stiffness of the underlying structure (column), as shown in Figures 3(c) and (d).

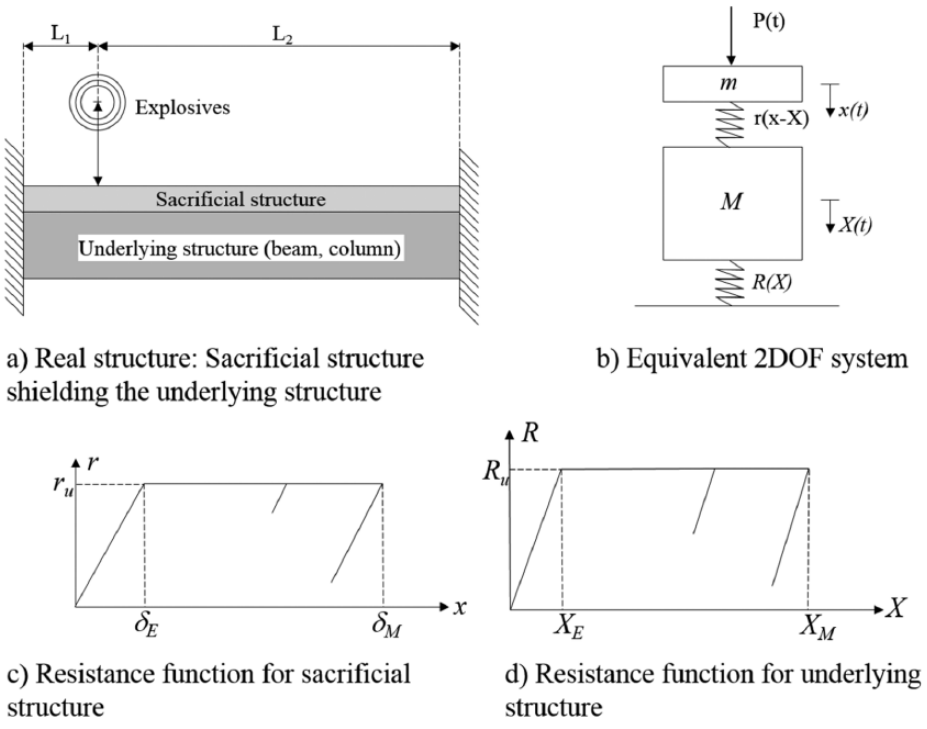

Figure 3. (a) Blast-loaded sacrificial structure mounted on underlying structure, (b) equivalent 2DOF system, (c) resistance function of sacrificial structure, and (d) resistance function of underlying structure.

The equations describing the dynamic response of the sacrificial structure and the underlying structure are shown in equations (4) and (5), respectively

$$m\ddot{x} + r\left(x\right) - X = P\left(t\right) \tag{4}$$

$$M\ddot{X} + R\left(X\right) - r\left(x - X\right) = 0 \tag{5}$$

$$\delta\left(t\right) = x\left(t\right) - X\left(t\right) \tag{6}$$

As suggested by Fujikura et al. (2008), we studied our high-resolution FE results in order to improve our understanding of simplified models, particularly by considering the ductility and absorbable energy of the two resistance functions. The following study comprises a comparative investigation of a structural member shielded with a sacrificial structure using (a) FE analysis, and (b) the 2DOF/SDOF analytical approach.

Blast performance of all-metal rectangular honeycomb sandwich elements

The all-metal sacrificial sandwich structure has rectangular honeycomb cells with dimensions 9.1 cm × 10.16 cm × 12.7 cm, as shown in Figure 2(b). The sandwich front plate and the core plates have different thicknesses, t_f and t_c, respectively, as also annotated in Figure 2(b).

Table 3. Thickness of front and core plates.

Honeycomb design	Front flange thickness t_f (cm)	Core plate thickness t_c (cm)	Relative mass $\mu = m_c/m_f$
Design 1	1.27	0.87	1.14
Design 2	2.29	0.62	0.46
Design 3	3.3	0.38	0.19

Three honeycomb designs of t_c/t_f ratio, that is, Designs 1–3, are explored covering a wide range of potential sacrificial honeycomb cell designs. Design 3 has a thick front face and thin core plates, while Design 1 consists of a thin front face and thick core plates, as shown in Table 3.

Elastic response of sacrificial cells and underlying structure (Impulse Level 1)

The impulse levels are determined by studying the kinetic energy (*KE*), as shown in equation (7)

$$KE = \frac{1}{2}mv^2 \tag{7}$$

where m and v are the mass and velocity of the object, respectively. The incremental change of *KE* is caused by change in momentum Δp, which is the impulse I, as shown in equation (8)

$$\mathrm{d}KE = I = \Delta p = m\left(v_2 - v_1\right) \tag{8}$$

where the unit on both sides of equation (8) is (Nm = J). The kinetic energy is then

$$KE = \frac{m}{2}\left(v_2^2 - v_1^2\right) \tag{9}$$

If the initial velocity is set to be zero (since the column did not move before applying the blast load), equation (9) becomes equation (7).

Equation (7) is accurate for a rigid body, while for a deformable body, elastic and plastic strain energy (as well as heat transfer) also affect the system energetics, leading to equation (1). Particularly for large blast events, mass becomes the dominant parameter in the response of the blast-loaded component, while energy absorption, through elastic or plastic deformations, is relatively small (Su et al., 1995). The change in momentum results in incremental change of kinetic energy, as shown in equation (7). If the impulsively loaded structure survives and stays stable, it vibrates elastically within a relatively short time while the *KE* decreases toward zero. In the following, we will discuss the change in *KE* as a result of applying Impulse Levels 1, 2, and 3.

Equation (1) can be interpreted further by multiplying both the nominator and denominator of the right-hand side by mass m and then replacing the product mv by the impulse I

$$KE = \frac{I^2}{2m} \tag{10}$$

As introduced above, Impulse Level 1 is characterized by elastic structural response. The reflected pressure and impulse acting on the target surface of the column move the front face of the sacrificial structure, the sandwich core, as well as the column (i.e. the underlying structure). The kinetic energy/area (*KE*) caused by the blast loading sees immediate momentum resistance,

that is, balances the momentum/area I (impulse). Using momentum conservation, the total kinetic energy/area corresponding to Impulse Level 1 (KE_1) is expressed by equation (11). Front face, core plate, and underlying structure (column) are allowed to move with different velocities

$$KE_1 = \frac{I_f^2}{2m_f} + \frac{I_c^2}{2m_c} + \frac{I_{col}^2}{2M_{col}} \tag{11}$$

where I is the impulse, m and M are the masses, and the subscripts f, c, and col stand for front face, core, and column (underlying structure), respectively.

Partial densification of the sacrificial cells (Impulse Level 2)

Impulse Level 2 is characterized by partial densification of the sandwich core. The rectangular honeycomb structure deforms up to full densification of the honeycomb cells. Once energy has been absorbed by crushing of the honeycomb core, the front face and core plates experience the same impulse. The velocity of the underlying structure is smaller. By momentum conservation, the KE/area corresponding to Impulse Level 2 up to full densification is expressed by equation (12)

$$KE_2 = \frac{I_{f=c}^2}{2}\left(\frac{1}{m_f} + \frac{1}{m_c}\right) + \frac{I_{col}^2}{2M_{col}} \tag{12}$$

The energy absorbed by densification is obtained by subtracting equation (11) from equation (12), $KE_2 - KE_1$.

In our FE model, the front face plate and web plates are discretized using elements of 2.5 cm side length. The web plate width is modeled by six elements which allow accurate representation of plate buckling. The front face plate has 20 elements over the width, as shown in Figure 2(a).

Front face and front flange time-dependent displacement due to impulsive loading is tracked and documented in the following paragraphs.

The dynamic response of sacrificial cells and underlying structure (column) are monitored as the front face plate of the all-metal sacrificial cells is loaded by a peak impulse of 0.091 MPa s measured at charge level 121.91 cm above the top ground surface (TGS). The peak lateral displacement of the front face plate is measured as 15.37, 15.75, and 20.32 cm for sacrificial Design 1, Design 2, and Design 3, respectively (Figure 4, left). The permanent displacement is 14.73, 15.37, and 19.55 cm, respectively. The measuring point is marked in the inserted sketch in Figure 4. The total displacement of the front face comprises densification of the all-metal sacrificial honeycomb cells as well as deformation and rigid body motion of the underlying structure.

The maximum permanent displacement of Design 3 varies significantly from Design 1 and Design 2. The different response is due to plate buckling of the thin honeycomb core plates in Design 3 under the corresponding blast load level, while the honeycomb core plates of Design 1 and Design 2 do not yet show this instability. The front face displacement of Design 2 is only slightly larger than in Design 1.

Honeycomb Design 3 shows the largest displacement of the front face plate among Designs 1–3 (Figure 4, left). Larger reflected pressure and impulse would cause full densification of Design 3 prior to Designs 1 and 2. Full densification of the sacrificial cells lets the pressure load to be directly transferred into the underlying structure (i.e. the gravity load–carrying column section). It is concluded that the sacrificial cell design which just precludes full densification when subjected

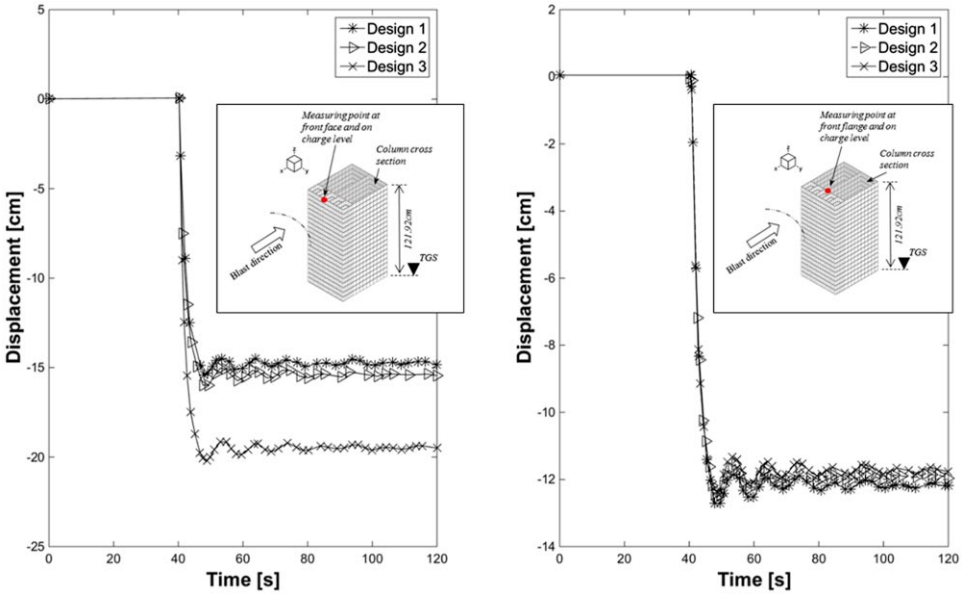

Figure 4. Comparison of sacrificial cell Designs 1–3 when subjected to reflected impulse $I = 0.091$ MPa s—Left: front face displacement of all-metal rectangular honeycomb cells; right: front flange (underlying structure) displacement shielded by all-metal rectangular honeycomb cells.

to a certain charge size constitutes the optimum design for just this charge size. Accordingly, the optimized sacrificial cell design (for a specific charge size) has a corresponding relative mass μ, as shown in Figure 5 (right). A smaller μ would result in thinner core plates and hence in less strain energy absorption through buckling of the core webs. A larger μ would result in thicker core plates and thinner front face plate which causes the front face plate to bend into the hollow space of the honeycomb cells, as shown in Figure 5 (left).

A thinner front face plate than in sacrificial cell Design 1 (see Table 3) makes the honeycomb design ineffective since tearing of the front face would cause blast pressure to enter the hollow honeycomb cells and load the sacrificial core locally. The thick continuous curve in Figure 5 (right) represents the optimum design for one specific load case (i.e. reflected pressure and impulse). The x-axis is the relative mass, and the y-axis represents the absorbed energy. The optimized protection, that is, maximum protection capacity due to the sacrificial structure, exists when full densification (compaction) of the sacrificial all-metal honeycomb cell structure is just prevented. Compaction of the honeycomb cells is triggered by out-of-plane buckling of the core plates. The broken lines in Figure 5 (right) represent the shift of optimized design of the sandwich element depending on the charge level. The optimized design ranges between small μ-design characterized by core plate buckling and large μ-design characterized by front face bending, which is less energy absorbent, as indicated by the decrease in achievable maximum energy absorption in Figure 5 (right).

However, the front flange, that is, the underlying structure, displacement provides insights into the level of protection of the underlying structure through sacrificial cell Designs 1–3. The lateral displacement varies only slightly among Designs 1–3, as shown in Figure 4 (right). From this result, we understand that the relative mass μ, being an important parameter for the blast design of

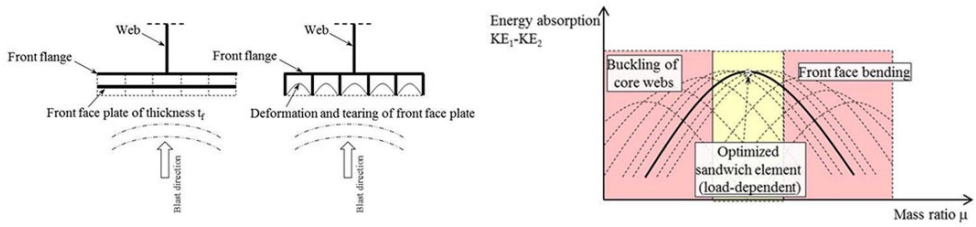

Figure 5. Left: sacrificial cell deformation for very small relative mass μ (left) and very large relative mass μ (right); right: load-dependent optimized sandwich plate for most efficient energy absorption (Rutner, 2012).

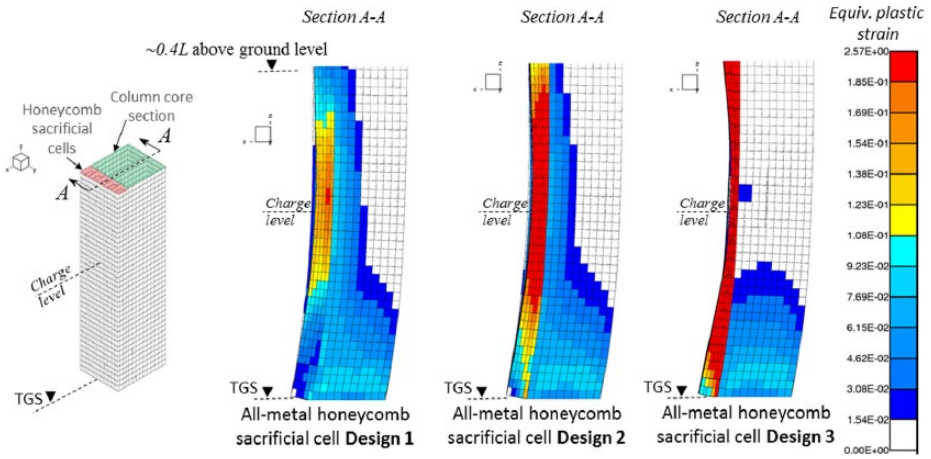

Figure 6. Equivalent plastic strain contour plots in all-metal rectangular honeycomb cells of Designs 1–3; maximum reflected impulse $I = 0.091$ MPa s.

sacrificial cell panels (Hutchinson and Xue, 2005), does not significantly affect the protection capacity of sacrificial cell structures mounted on an underlying structure.

Strain contour plots provide information about the force flow and potential damage in the sacrificial cell and the underlying structure. The honeycomb sacrificial cell section and the axial load–carrying column core section are annotated in Figure 6. Figure 6 shows the column with the three different sacrificial cell structure Designs 1–3 subjected to identical blast loading, that is, a maximum reflected impulse of 0.091 MPa s. Figure 6 shows the column from the ground surface up to a height of about $0.4L$ (L being the length of the column) in isometric view and a cut through the vertical symmetry plane. Design 3 honeycomb cells densify more than the honeycomb Designs 1 and 2 under the identical impulsive loading. The strain contours reveal the level of protection of the underlying structure through the sacrificial structure. The Design 3 sacrificial honeycombs absorb more energy than Designs 1 and 2. It is recognized that a potential failure mode of base shear-off is not being attenuated by variation of sacrificial cell Designs 1–3. The plastic strain levels at the column bottom consistently amount to about 8% equivalent plastic strain.

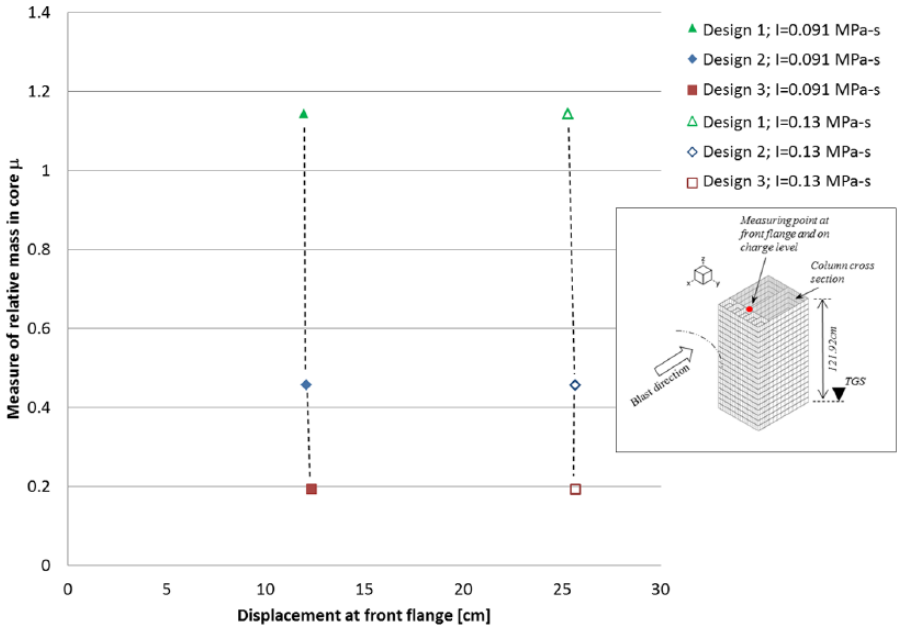

Figure 7. Relative mass plotted over the front flange displacement for all-metal honeycomb sacrificial cell Designs 1–3; maximum reflected impulse $I = 0.091$ MPa s and $I = 0.133$ MPa s.

Full densification of sacrificial cells (Impulse Level 3)

The kinetic energy KE_2 of equation (12), which remains after full densification of the honeycomb cells, loads the underlying structure, that is, the gravity load–carrying column section, directly. Hence, two effects are identified as main mechanisms contributing to the dynamic column response and to the level of blast resistance:

- The energy absorption through densification of sacrificial cells structure, as discussed in the section "Partial densification of the sacrificial cells (Impulse Level 2)";
- The momentum resistance provided by the mass of sacrificial structure and underlying structure.

Figure 7 shows the front flange displacement, that is, the displacement of the underlying structure, when subjected to two different blast load levels, that is, maximum reflected impulse 0.091 or 0.133 MPa s. The front flange displaces by a consistent value among Designs 1–3.

The plastic strain contour plots of the three sacrificial cell designs, Designs 1–3, mounted on the air-filled column (i.e. underlying structure), show only small variation of strain contours in the web (section A-A) among the three designs when subjected to a peak reflected impulse of $I = 0.133$ MPa s. The ratio of absorbable energy through densification and released blast energy decreases as the charge size increases. The contour plots demonstrate that the base shear is the governing failure mode (Figure 8).

The sacrificial structure types investigated so far, that is, Designs 1–3, enable blast protection through energy absorption. However, following equation (9), increasing the mass reduces

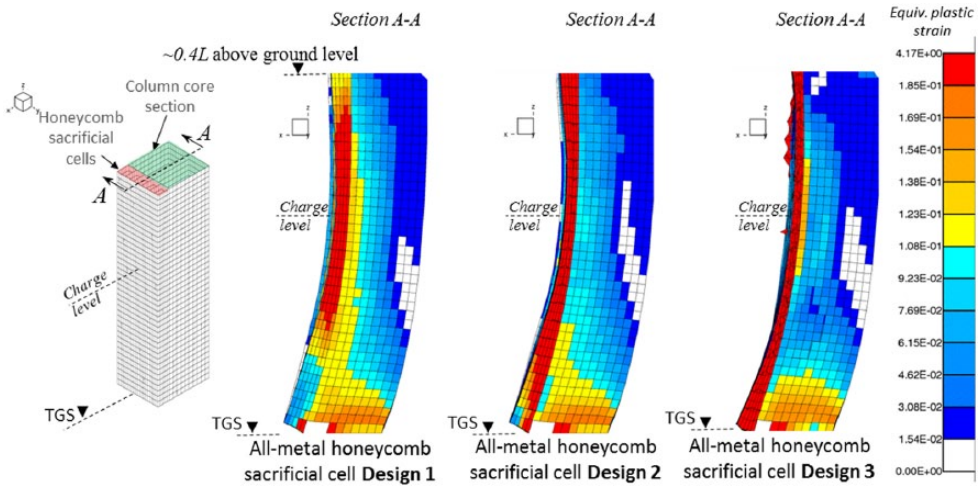

Figure 8. Equivalent plastic strain contour plots of the air-filled column (underlying structure) shielded by the sacrificial cell Designs 1–3 subjected to peak reflected impulse $I = 0.133$ MPa s.

the kinetic energy by providing increased momentum resistance. In the following, the dynamic response of several sacrificial structures of the same outer dimensions but with different mass is investigated when subjected to three different blast load levels represented by the peak reflected impulses 0.049, 0.091, and 0.133 MPa s. The sacrificial structure designs are listed in Table 4.

At Impulse Level 3, characterized by full densification, the mass of the sacrificial structure, m_{sac}, moves with the same velocity as the mass of the underlying structure (column), M_{col}. The kinetic energy KE_3 is given by equation (13).

From equation (9) it becomes obvious that adding mass and thus increasing the momentum resistance constitute an effective measure to reduce the kinetic energy of the underlying structure

$$KE_3 = \frac{I^2}{2\left(m_{sac} + M_{col}\right)} \tag{13}$$

Equation (13) shows the mass of the sacrificial and the underlying structure, m_{sac} and M_{col}, respectively, in the denominator. In the following, we will investigate and quantify the effect of mass embedded in sacrificial structure and underlying structure on the dynamic response behavior of the underlying structure. As long as the added mass causing momentum resistance balances the kinetic energy, the underlying structure is stable. Hence, momentum resistance might even resist large reflected blast pressure and impulse, at transient load levels where energy absorption of light-weight cells is no longer effective.

Comparison of absorbable energy of sacrificial and underlying structure

Upon full densification of the sacrificial cell structure, the initial 2DOF system, as shown in Figure 3, becomes a SDOF system. The energy to be absorbed by elastic and plastic strain energy capacity

Table 4. Mass of the sacrificial structure and mass of total column section (in parentheses).

Sacrificial structure design	Mass (kg/m)
Structural steel infill	439.24 (1055.45)
Foam concrete infill	125.96 (742.16)
Honeycomb Design 3	133.6 (749.81)
Honeycomb Design 2	111.31 (727.51)
Honeycomb Design 1	91.49 (707.70)

of sacrificial and underlying structure is shown by equation (13). From equation (1), the ductility D of the underlying structure is

$$D = \frac{X_M}{X_E} = \frac{1}{2}\left(\frac{I^2}{K_{LM} M R_u X_E} + 1\right) \tag{14}$$

Hence, the impulse limit based on ductility is shown in equation (15)

$$I_D = \sqrt{(2D-1) K_{LM} M R_u X_E} \tag{15}$$

Similarly, for the sacrificial structure with ductility $d = \delta_M/\delta_E$, the impulse limit for the sacrificial cladding is

$$i_d = \sqrt{(2d-1) k_{LM} m r_u \delta_E} \tag{16}$$

where k_{LM} is the load–mass factor for the sacrificial structure. Finally, the ratio of impulse limits is

$$\frac{I_D}{i_d} = \sqrt{\frac{(2D-1) K_{LM} M R_u X_E}{(2d-1) k_{LM} m r_u \delta_E}} \tag{17}$$

The ratio of impulse limits plotted versus the mass of sacrificial cells is shown in Figure 9. While the ratio of impulse limits is in the order of 6–7 for the lightweight honeycomb sacrificial design, it drops significantly to below 2 for very massive sacrificial structure design, that is, the solid steel plate.

When the sacrificial structure is an air-filled metal honeycomb structure, the ratio of impulse limits is large, indicating the very superior strain energy capacity of the underlying structure compared with the sacrificial structure, marking lightweight honeycomb cells an unpractical protection measure for high impulsive loading. However, if the sacrificial structure is massive, for example, a solid steel plate, the ratio of impulse limits decreases, making a more massive sacrificial structure a better design choice. One data point in Figure 9 is the air-filled metal honeycomb sacrificial structure shielding the air-filled column (Case 4 in Table 2). For this case, the resistance, mass, and elastic displacement ratios are as follows: $R_u/r_u = 55.92$, $M/m = 4.61$, and $X_E/\delta_E = 0.146$. Accordingly, the ratio of impulse limits $I_D/i_d = 6.13$, meaning that the column, that is, the underlying structure, can absorb 6.13 times more elastic–plastic strain energy than the sacrificial cladding when subjected to impulsive loading. Table 5 shows 17 different column designs (selected from the original 30 cases analyzed by FE modeling as listed in Table 2)

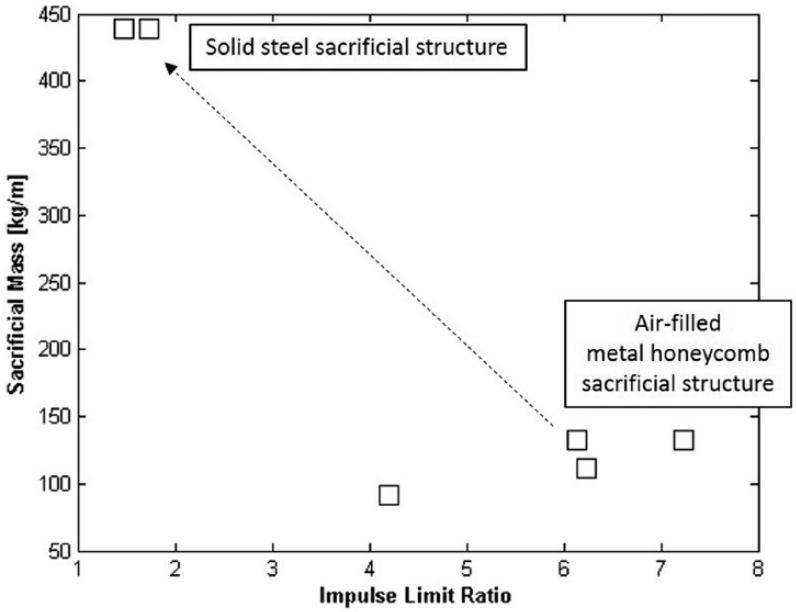

Figure 9. Mass of sacrificial structure plotted against impulse limit ratio.

investigated using the equivalent SDOF system. The second to last column in Table 5 lists the ratio of impulse limits.

Figure 10 plots the total mass per length, that is, mass of the sacrificial structure (m_{sac}) and mass of the underlying structure (M_{col}), over the front flange displacement. Structural steel infill provides approximately 3.5 times more mass than the all-metal honeycomb Design 3 and correspondingly results in smaller displacement. For all three impulsive load levels investigated, that is, maximum impulse = 0.049, 0.091, and 0.133 MPa s, the front flange (i.e. the underlying structure) shows the smallest displacement when the sacrificial structure is made of solid steel (see Figure 10), while the column shielded by foam concrete displaces more than the same column shielded by honeycomb cell Design 3.

The momentum resistance generated by the massive sacrificial steel structure drives down the residual kinetic energy of the front flange, hence protecting the underlying structure. The honeycomb Design 3 provides a higher level of protection to the underlying structure than the sacrificial structure filled with foam concrete infill material.

The mass-displacement slopes are sketched in Figure 10 by broken lines to visualize the sacrificial mass effect on the underlying structure displacement for the three load levels investigated. The gradient of the broken line averaging the data of the same load level becomes less steep with increasing transient load level.

Figure 11 reveals the effect of sacrificial structure mass on the strain contours in the column, that is, the underlying structure. Left, middle, and right plots compare the equivalent plastic strain distribution induced by two different reflected impulse levels. Reflected impulse of 0.049 MPa s causes densification of the all-metal honeycomb cell Design 3 (Figure 11, left). The energy absorption of the honeycomb cells causes the gravity load–carrying column cross section (i.e. the

Table 5. Selected cases of column design for SDOF analysis.

Case	Sacrificial structure	Core column	X_M (FE) (m)	X_M (SDOF) (m)	M_{Total} (kg/m)	$N_{sacrificial}$ (kg/m)	M_{core} (kg/m)	I (MPa s)	I_D/i_d	K_{LM}
1	Air-filled (Design 3)	Concrete-filled	0.017	0.023	945.910	133.600	812.310	0.049	7.030	0.455
3	Solid steel	Concrete-filled	0.012	0.014	1251.550	439.240	812.310	0.049	1.740	0.377
4	Air-filled (Design 2)	Air-filled	0.033	0.029	749.800	133.600	616.200	0.049	6.130	0.294
6	Solid steel	Air-filled	0.020	0.017	1055.440	439.240	616.200	0.049	1.477	0.277
7	Air-filled (Design 1)	Air-filled	0.130	0.111	707.700	91.500	616.200	0.091	4.200	0.283
8	Air-filled (Design 2)	Air-filled	0.124	0 104	727.510	111.310	616.200	0.091	6.228	0.275
9	Air-filled (Design3)	Air-filled	0 124	0.097	749.803	133.603	616.200	0 091	6.130	0.257
10	Air-filled (Design 3)	Concrete-filled	0.060	0.075	945.910	133.600	812.310	0.091	7.227	0.412
12	Solid steel	Concrete-filled	0.039	0.043	1251.550	439.240	812.310	0.091	1.740	0.370
15	Solid steel	Air-filled	0.076	0.054	1055.440	439.240	616.200	0 091	1.477	0.235
16	–	Air-filled	0.182	0.159	616.200	–	616.200	0.091	–	0.289
18	–	Concrete-filled	0.077	0.118	812.310	–	812.310	0.091	–	0.509
19	Air-filled (Design 3)	Air-filled	0.124	0.097	749.803	133.603	616.200	0 091	6.130	0.258
24	Air-filled (Design 3)	Air-filled	0.262	0.196	749.803	133.603	616.200	0.133	6.130	0.246
25	Air-filled (Design 3)	Concrete-filled	0.131	0.151	945.913	133.603	812.310	0.133	7.227	0.379
27	Solid steel	Concrete-filled	0.079	0.087	1251.550	439.240	812.310	0.133	1.741	0.361
30	Air-filled (Design 3)	Air-filled	0.147	0.109	1055.440	439 240	616.200	0.133	1.477	0.243

SDOF: single-degree-of-freedom.

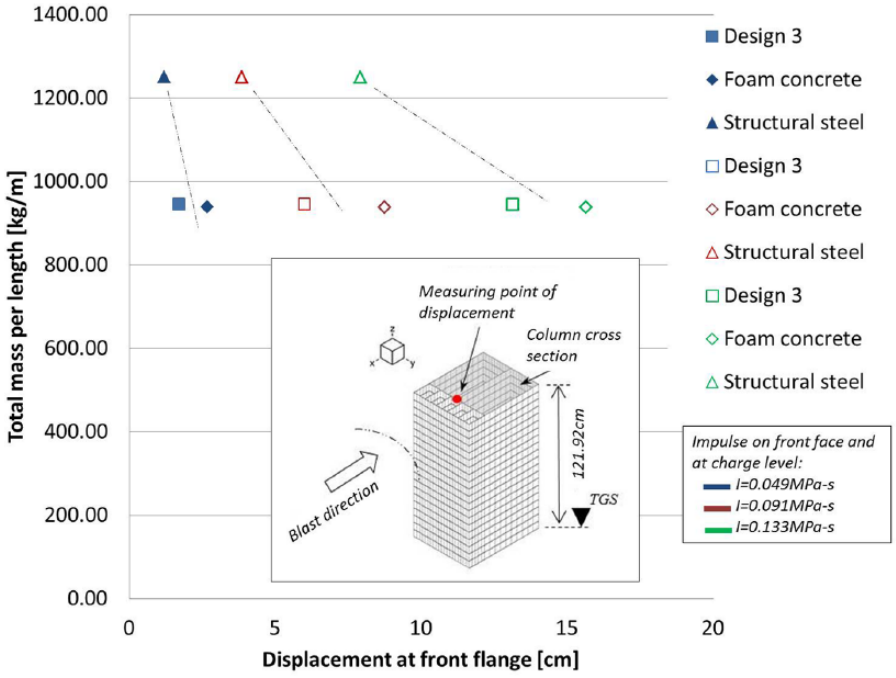

Figure 10. Mass of sacrificial cells plotted against front flange displacement.

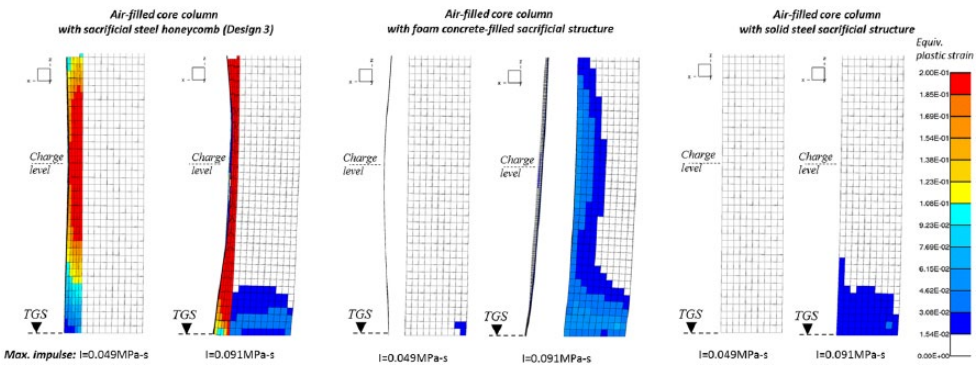

Figure 11. Effect of mass of sacrificial cells on the strain contours in the underlying structure (i.e. air-filled column)—Left: air-filled rectangular honeycomb cells (Design 3); middle: foam concrete infill material; right: sacrificial solid steel plate mounted on the underlying structure.

underlying structure) to stay completely elastic. An increased charge load generating a reflected impulse of 0.091 MPa s causes densification of the sacrificial cells, the column cross section at charge level still being elastic. However, there is plastic strain in the order of 5% at the column bottom.

When the underlying structure, that is, the column core section, is shielded by a sacrificial foam concrete infill covered by a 2.54-cm-thick steel plate at the front face (as sketched out in Figure 2, right), the column core section shows slight plastic strain at the column bottom when loaded by a maximum reflected impulse of 0.049 MPa s (Figure 11, middle). When the blast load is increased generating a reflected impulse of 0.091 MPa s, the column core section shows plastic strain distributed over the whole column height. This demonstrates that using foam concrete as sacrificial cell design is not as protective as the honeycomb cell Design 3. In both load cases, the rebound effect causes the 2.54-cm-thick steel plate to fly off after full densification of the porous foam concrete structure.

When the sacrificial structure is solid steel, that is, the column core section is now shielded by a 12.7-cm-thick steel plate, the strain in the column core section is entirely elastic when loaded by an impulse of 0.049 MPa s. Under increased reflected impulse of 0.091 MPa s, the column bottom shows minor strain of up to 3% (Figure 11, right).

It is concluded that mass added to the sacrificial structure helps to decrease displacement and plastic strain in the underlying structure, as demonstrated in Figures 10 and 11. Mass is identified as one of the governing parameters in protective design of structural members subjected to blast loading.

In the extreme case of very large charges (reflected pressure and impulse), mass should play the dominant role in the protection strategy of structures subjected to blast. So far, the effect of mass embedded in sacrificial cells which are mounted on the underlying structure has been discussed above. In the following, we will investigate the effect of mass of the underlying structure, M_{col}, on the dynamic response. The column core cross section, as shown in Figure 2, is filled in one case with normal concrete and in another case with foam concrete, and in a third case, the column section remains air-filled. Additionally, each of the three cases is investigated with and without sacrificial cells. The sacrificial cell design selected is the honeycomb Design 3, as specified in Table 3.

All column designs investigated in the following are subjected to the same impulsive loading, that is, the maximum reflected impulse 0.091 MPa s acting on the column target surface at charge level. The relationship between the mass of the column and permanent lateral displacement is evaluated for all cases investigated. The displacement is measured at the front flange and annotated in the inserted sketch.

The symbols used for normal concrete infill, foam concrete infill, and air-filled column design are triangle, square, and diamond, respectively. The solid symbols mark the designs with sacrificial cells, while the hollow symbols mark the designs without sacrificial cells. The contribution of the mass of the underlying structure (momentum resistance) on the permanent displacement (at charge level) as well as the effect of sacrificial cells on reducing the displacement is quantified separately. Clearly, the mass of the underlying structure affects the permanent lateral displacement. It is obvious that if the contribution of lightweight sacrificial cells (in this case, honeycomb cell Design 3) on the total response (displacement) becomes larger, the less massive the underlying structure is. The displacement reduction gained by the sacrificial cells is annotated in Figure 12. However, for massive underlying structures, the contributing effect of lightweight sacrificial cells becomes nearly negligible, as shown in Figure 12.

Figure 13 shows the strain contours of the column core section in the vertical cut along the symmetry plane of the column cross section. Left, middle, and right plots compare the equivalent plastic strain contours in the underlying structure of different mass levels (see Table 6) with and without lightweight honeycomb cells of Design 3 (as specified in Table 3). The column is loaded with a maximum reflected impulse of 0.091 MPa s at charge level. Figure 13 (left) compares the air-filled column core with and without honeycomb cells of Design 3. There is a reduction in the equivalent plastic strain adjacent to the bottom of the column from about 14% strain to 9% strain

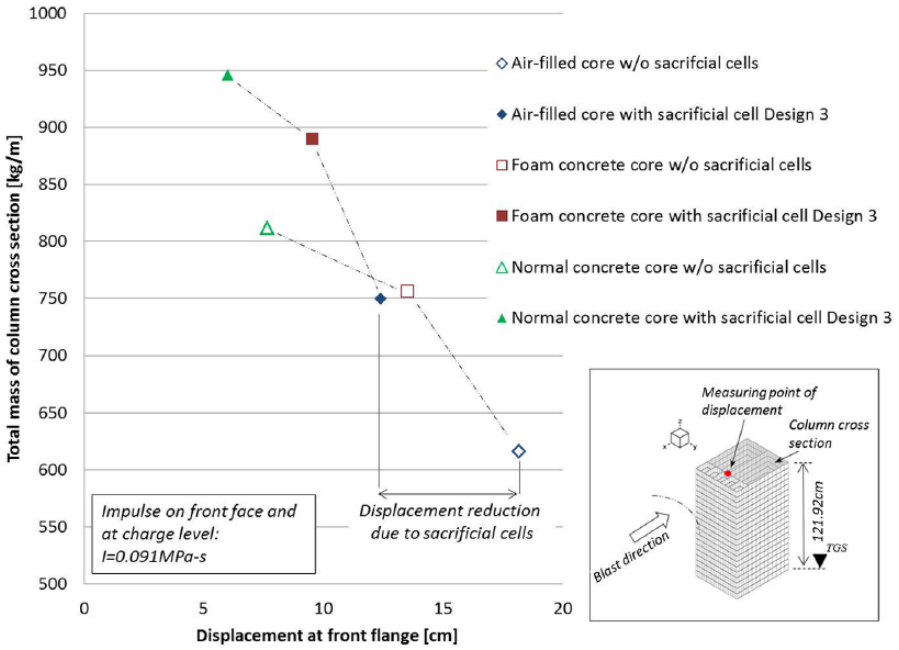

Figure 12. Effect of mass of the underlying structure on the permanent displacement of the front flange.

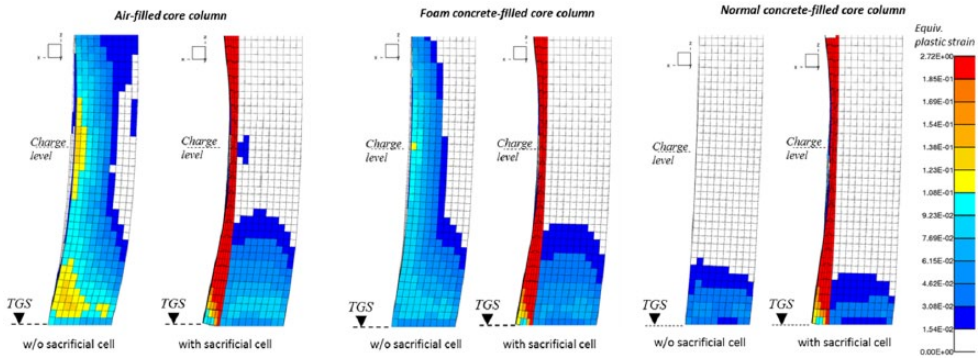

Figure 13. Effect of mass of the underlying structure on the strain contours in the underlying structure—Left: air-filled column section; middle: foam concrete-filled column core section; right: normal concrete-filled column cross section; plastic strain contours of the column member without and with honeycomb sacrificial cells (Design 3); maximum reflected impulse on the front face at charge level is 0.091 MPa s.

due to the energy absorption of the sacrificial cells, as shown in the section cut along the symmetry plane. The strain in the web of the gravity load–carrying core cross section is significantly reduced from 14% plastic strain to elastic strain.

Table 6. Mass per length of the underlying structure without sacrificial structure and total mass per length in parentheses.

Column core infill material	Mass of underlying structure, M_{col}, and total mass per length (kg/m)
Normal concrete	812.31 (945.92)
Foam concrete	756.28 (889.88)
Air-filled	616.20 (749.81)

Figure 13 (middle) shows the column filled with foam concrete with and without honeycomb sacrificial cell Design 3 when subjected to a maximum reflected impulse of 0.091 MPa s. The strain at load level can be reduced by the sacrificial cells from 12% plastic strain to elastic strain level. The strain in the column web at the base is only marginally reduced from 9% to about 8%. Hence, the shear-off failure mode is expected to be the governing failure mode when the charge load is increased. Figure 13 (right) shows the column filled with normal concrete with and without honeycomb sacrificial cells of Design 3. The strain at charge level is elastic even at the column without sacrificial cells. There is plastic strain in the column web at the base of the order of about 6%, which is reduced by applying honeycomb sacrificial cells (Design 3) to about 4%. Comparison of the strain contours of the underlying structure without sacrificial cells in Figure 13 allows quantification of the effect of infill material mass on the underlying structure with regard to plastic strain distribution. The 14% maximum strain in the air-filled column is reduced to elastic strain levels due to filling the column with normal concrete, which emphasizes the importance of mass and momentum resistance in blast-resistant design.

Discussion of results obtained through FE analysis and equivalent SDOF analysis

Table 2 lists the 30 column design cases investigated by FE modeling, while 17 cases out of these 30 cases have been modeled using equivalent SDOF systems, as listed in Table 5. Figure 14 lists the resulting permanent lateral displacement gained through FE and SDOF analyses and the respective total mass. The three diagrams in Figure 14 summarize the data for the three reflected impulse levels investigated, that is, $I = 0.049$, 0.091, and 0.13 MPa s, respectively. For each design case, the FE and the SDOF analyses results are shown by a star and a triangle, respectively. The SDOF analysis provides results which differ from the high-resolution FE results of the order of a few centimeters. Reasons for this inaccuracy and potential prevention are discussed in the following.

In the equivalent SDOF approach, the permanent displacement depends on load–mass factor K_{LM}, mass M, and resistance function R_u, as shown in equation (14). While mass and resistance function can be explicitly determined using basic structural analysis, that is, well-defined boundary conditions, the determination of the load–mass factor K_{LM} is not straight forward. In our comparative FE/SDOF analysis, the permanent displacement of the FE analysis is considered the reference value. The K_{LM} value applied in the SDOF system is changed to match the FE result. Figure 15 plots the K_{LM} values against the mass of the underlying structure. Underlying structures of lower mass require a K_{LM} value between 0.2 and 0.3, while a more massive underlying structure of the same outer dimensions requires a K_{LM} in the order of about 0.34–0.45. The K_{LM} factor for the clamped girder loaded by a centric single load is 0.33, while the same system loaded by a uniform load results in a K_{LM} of 0.66 (Cormie et al., 2009). The following provide some thoughts about this:

Stiffening up the column, which is achieved through concrete infill of the core column, for example, Cases 1 and 10 of Table 5, causes a significant increase in the K_{LM} value. We could argue that, consistent with equations (2) and (3), the mass is significantly increased, hence leading to a

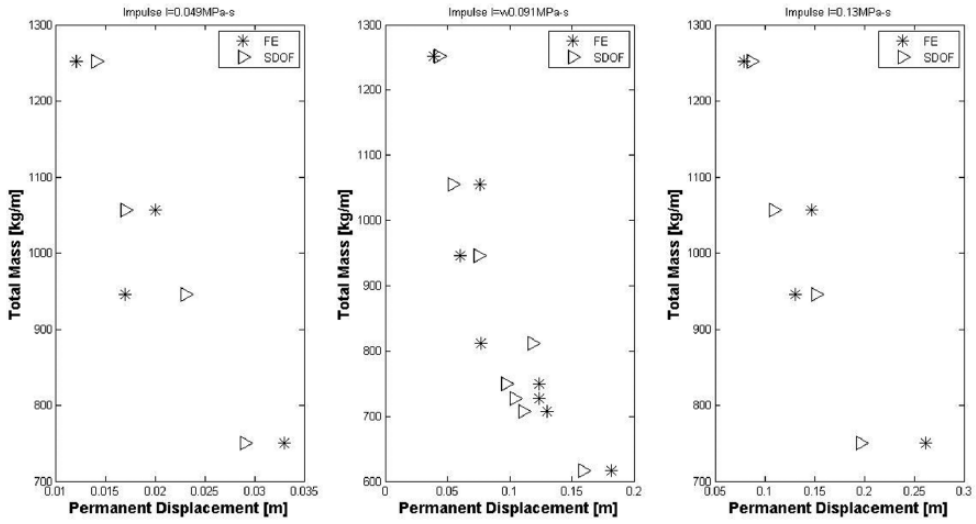

Figure 14. Comparison of results gained through FE analysis and SDOF system analysis: Permanent lateral displacement of the column at charge level.

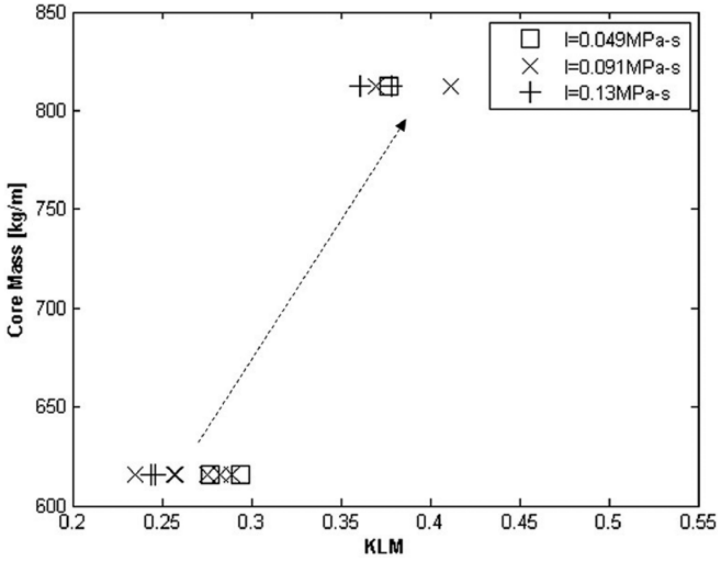

Figure 15. The mass of the underlying structure (column) versus the load–mass factor $K_{LM.}$

larger K_M and hence a larger K_{LM}. Furthermore, a stiffer girder results in a more parabolically-shaped deformation than a triangular-shaped one, increasing $\varphi(x)$, which is square powered in equation (2). On the other hand, adding mass into the sacrificial structure does not increase the K_{LM}

value, as shown with Cases 6 or 15. Accordingly, we conclude that the K_{LM} value depends on the mobilized mass and stiffness resistance of the underlying structure. Building a test matrix to explore the connections and interdependencies further would be valuable. The dependence of K_{LM} on the core mass is shown in Figure 15. We notice that the correlation is (nearly) independent of the reflected impulse level.

Duality of energy absorption and inertial effects

The optimized design of lightweight sacrificial cells is achieved when the blast load densifies the sacrificial cells, however does not reach full densification, hence providing the maximum energy absorption since at full densification of the cellular material any further loading is being transferred undiminished into the underlying structure. For larger explosive charges at close standoff, where the quantity of absorbable kinetic energy constitutes only a small fraction of the released blast energy, lightweight sacrificial cells are not a suitable structural hardening concept, as shown by the ratio of impulse limits I_D/i_d in the section "Blast Performance of All-Metal Rectangular Honeycomb Sandwich Elements". Lightweight sacrificial cells would require a crash zone of large dimensions to effectively accommodate the large pressure and protect the underlying structure. Significant inertial forces are not activated in lightweight sacrificial cell construction. The findings in this article indicate significant inertial resistance to the shock pressure wave. Mass located in the sacrificial section as well as column core section (underlying structure) provides protection primarily through activated inertial forces rather than through energy absorption and outperforms lightweight infill materials from a certain load level on. Comparing Cases 3 and 4 from Table 5 show that the choice of a massive solid steel sacrificial structure provides a ratio of impulse limits I_D/i_d of 1.74, emphasizing that the sacrificial structure contributes much more to the blast resistance of the column section, compared with the air-filled honeycomb sacrificial structure design of Case 4, where the core column dominates the blast-resistant capacity (I_D/i_d of 6.13). On the other hand, filling the core column with concrete, as shown in Case 1, increases the mass, hence increasing I_D/i_d and the effective K_{LM} value.

The duality of energy absorption and inertial effects lead to two different modes of protection as suggested by the two regions in Figure 16. With increasing transient load parameters, that is, reflected pressure and impulse, there is a transition from energy absorption to inertial effects governing the response and protection capacity of sacrificial cells. In order to achieve sufficient protection of the underlying structure, the infill material of sacrificial cells should be carefully selected. At low reflected pressure and impulse, lightweight air-filled material is an appropriate infill material since the kinetic energy induced in the target surface can be sufficiently/fully absorbed through sacrificial cell deformation. The crash zone should be designed large enough so that the sacrificial cells infill material does not fully densify before most of the energy is absorbed. Massive materials are appropriate to protect the underlying structure against larger impulsive load, as shown in the three-dimensional (3D) diagram of Figure 16. The mass in the sacrificial structure provides immediate momentum resistance. Fluid-filled foam, which combines energy absorption effects as well as inertial effects, constitutes a potential sacrificial cell infill material against mid-range pressure and impulse (Dawson et al., 2009).

An interrelation of the three parameters, mass, impulse, and displacement, which govern the blast response in the high impulse range when mass becomes the dominant parameter, is derived in the following. In order to investigate how the parameters impulse, displacement/deformation, and mass correlate with each other and in what range, all data obtained in the FE analyses in this study are plotted in a 3D diagram. The *x*-, *y*-, and *z*-axes of the diagram are permanent displacement in the blast direction, maximum impulse, and mass per length, respectively, as shown in

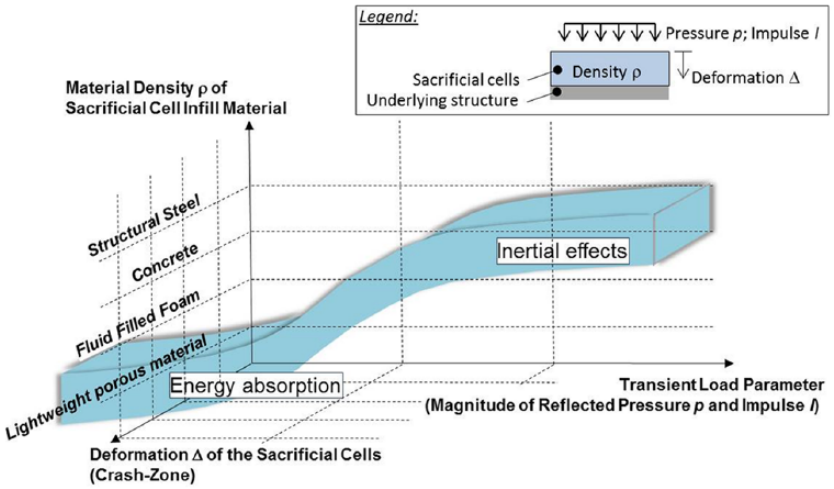

Figure 16. Duality of energy absorption and inertial effects.

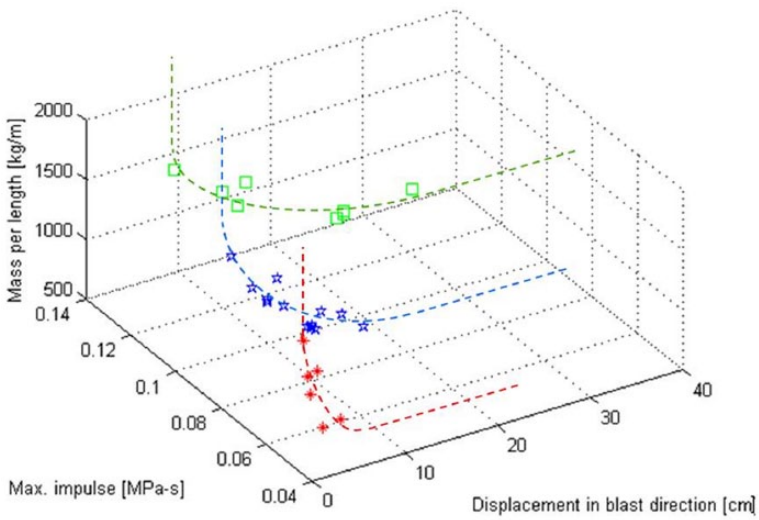

Figure 17. Governing parameters, that is, maximum reflected impulse, permanent displacement, and mass, representing structural member response.

Figure 17. Hence, the axes also represent the governing parameters of equation (1). The data obtained with low impulse level (reflected impulse = 0.049 MPa s) are shown as red stars, and the data due to medium and high impulse (reflected impulse = 0.091 and 0.133 MPa s, respectively) are plotted as blue pentagons and green squares. It is recognized that the data set per impulse level can be represented as a curve drawn into the diagram. Please note that the low impulse-generated data are stretched in the vertical direction relative to the high impulse-generated data,

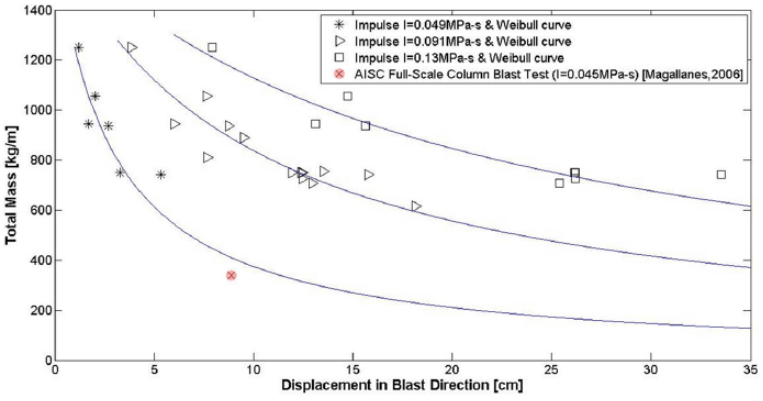

Figure 18. Governing parameters, that is, maximum impulse, displacement, and mass, representing structural member response.

which are stretched horizontally. This seems to be a generally valid observation. The scatter of the curves is very limited although significant changes in the cross section have been made, as discussed in previous sections, which is understood as a further confirmation that the governing parameters (which represent the axes of the 3D diagram) have been found. Obviously, the nonlinear response of a column subjected to blast can be predicted using a response surface which combines the curves shown in Figure 17. This response surface approach might open up a new perspective for the preliminary design of structural members of the same failure mode and optimization of blast-resistant design. A response surface defined in mathematical terms by the governing parameters would enable on-site vulnerability assessment of structural/mechanical members subjected to impulsive loading with high accuracy and in a very time-efficient manner. Further investigations are underway to determine whether this analytical methodology can be made to be quantitative criterion for use in protective design. Also, the authors are currently looking into incorporating boundary condition(s) as a fourth governing parameter, besides mass, impulse, and displacement (Rutner et al., 2008).

Validation of FE analysis

The response data achieved through FE modeling shown in Figure 17 are plotted in a two-dimensional diagram in Figure 18. Abscissa and ordinate show the mass of the column and the permanent displacement, while the reflected impulse level is annotated in the legend. The three data clouds with star, triangular, and square symbols correspond to the impulse levels applied, that is, 0.049, 0.091, and 0.133 MPa s, respectively. A best-fit polynomial approach is used to average each data cloud, represented by the continuous curves.

The AISC Full-Scale Column Blast Test (Magallanes et al., 2006) is added as a single data point, that is, the cross, in Figure 18. Figure 19 depicts the column and load characteristics as well as a top view of the test setup. The blast load is a 4000 lb TNT (Trinitrotoluene)-equivalent of Ammonium Nitrate/Fuel Oil charge at a standoff of 4.572 m. The charge level is 137.16 cm above ground. The charge shape is a 1.52-m-diameter cylinder of 1.473 m height. The column sees a reflected impulse of 0.0448 MPa s. The column flange is exposed to the charge direction at a skewed angle. The test column is a 14WF228 column which is set at both ends into reinforced

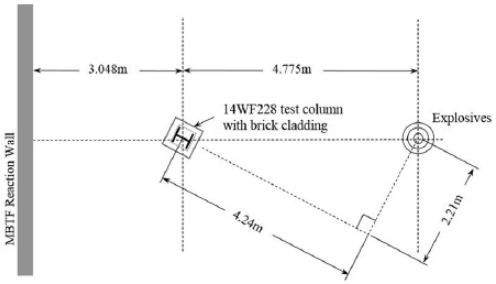

	Column	Length [m]	Mass [kg/m]	Refl. impulse [MPa-s]	Displacement @ charge level [cm]
AISC Blast Test	14WF228*	5.715	228	0.0448	8.89

* The column is surrounded by a brick cladding which does not add to the bending and shear stiffness of the column

Figure 19. AISC Large-Scale Blast Test (Magallanes et al., 2006).

foundations which are held in place by a reaction wall. The final permanent displacement in charge direction at charge level is 8.89 cm.

Furthermore, our comparative analysis comprising FE and SDOF analyses confirms the validity of the deformation limits as reported by Cormie et al. (2009).

Conclusion

The study presented herein had three main objectives, namely: (a) exploring the key parameters governing failure of a sacrificial honeycomb structure shielding a structural member using analytical SDOF/2DOF analysis and high-fidelity explicit FE analysis; (b) understanding and quantifying the protection capacity of a sacrificial honeycomb cell structure mounted on an underlying structure accounting for full densification of the sacrificial cells; and (c) investigating to what extent high-resolution FE analysis can be used to improve current SDOF system analysis approaches.

A honeycomb structure consisting of rectangular air-filled cells has been studied with respect to its protection capacity to shield an underlying structure. Three different designs of honeycomb cells have been investigated by varying the relative mass of core plates and front face plate.

An energy approach was used to describe the transition of kinetic energy activated during three stages, that is, elastic range, densification, and full densification of the sacrificial structure subjected to impulsive loading, demonstrating the transition from equivalent 2DOF to SDOF systems representing the nonlinear structural member response.

The relative mass μ was shown to be a relatively unimportant parameter in blast-resistant design of sacrificial structures once the sacrificial cells fully densify. However, the masses of the sacrificial structure and underlying structure were found to be the governing design parameters. The higher the impulsive loading, the lesser the effect of energy absorption and the larger the effect of mass on the dynamic response of the underlying structure through activation of momentum resistance. The findings indicated a duality of energy absorption and inertial effects in transient dynamics. A 3D design diagram has been developed where the clouds of response data establish a response surface representing the complex nonlinear response of structural members subjected to blast loading. This response surface approach might open up a new perspective for the preliminary design of structural members of the same failure mode. Further investigations are underway to: (a) prove whether this analytical methodology can be made a quantitative criterion for use in protective design; and (b) to find a mathematical approach to describe the response surface. Free-air blast test results were used for validation of the numerical results.

Comparative analysis using FE analysis and SDOF methods showed the need for a more accurate definition of the load–mass factor K_{LM}. Further studies are required to make the load–mass factor easier and more accurately predictable which would be very valuable for design.

The FE analysis confirmed the deformation limits established for SDOF system blast analysis.

Declaration of conflicting interests

The author(s) declared no potential conflicts of interest with respect to the research, authorship, and/or publication of this article.

Funding

The author(s) disclosed receipt of the following financial support for the research, authorship, and/or publication of this article: MPR was funded by the German Research Foundation (DFG) during the initial two years of this research (Ru 931/2-1, and Ru 931/2-2). The financial support is greatly appreciated.

References

Biggs JM (1964) *Introduction to Structural Dynamics*. New York: McGraw-Hill.

Cormie D, Mays G and Smith P (2009) *Blast Effects on Buildings* (2nd edn). London: Thomas Telford.

Dawson MA, McKinley GH and Gibson LJ (2009) The dynamic compressive response of an open-cell foam impregnated with a non-Newtonian fluid. *Journal of Applied Mechanics* 76(6): 061011.

Ehrgott JQ (1973) Investigation of the static uniaxial strain and triaxial shear response of cellular concrete. Final report, Army Engineer Waterways Experiment Station, Vicksburg, MS, May.

Fleck N and Deshpande VS (2004) The resistance of clamped sandwich beams to shock loading. *Journal of Applied Mechanics* 71: 386–401.

Fujikura S and Bruneau M (2012) Dynamic analysis of multihazard-resistant bridge piers having concrete-filled steel tube under blast loading. *Journal of Bridge Engineering: ASCE* 17(2): 249–258.

Fujikura S, Bruneau M and Lopez-Garcia D (2008) Experimental investigation of multihazard resistant bridge piers having concrete-filled steel tube under blast loading, journal of bridge engineering. *Journal of Bridge Engineering: ASCE* 13(6): 586–594.

Gibson LJ and Ashby MF (1997) *Cellular Solids—Structure and Properties* (2nd edn). Cambridge: Cambridge University Press.

Hutchinson JW and Xue Z (2005) Metal sandwich plates optimized for pressure impulses. *International Journal of Mechanical Sciences* 47: 545–569.

Hyde DW (1992) *CONWEP-Conventional weapons effects programme*. USAEWES.

Kingery CN and Bulmash G (1984) *Airblast parameters from TNT spherical air burst and hemispherical surface burst*. ARBRL-TR-02555, US Army Armament Research and Development Center, BRL, Aberdeen Proving Ground, Maryland, USA.

Magallanes JM, Martinez R and Koenig JW (2006) *Experimental results of the AISC full-scale column blast test*. TR-06-20.2, Contract no. KC-05-27.2, Prepared for the American Institute of Steel Construction, Chicago, IL, March.

Mould JC and Levine HS (1994) A rate-dependent three invariant softening model for concrete. *Studies in Applied Mechanics* 35: 11–38.

Rutner M (2012) *Load-Carrying Columns Subjected to Impulsive Loading—Protection Technology in High-Speed Dynamics, Habilitation*. Munich: Technical University Munich.

Rutner M, Mensinger M and Trometer S (2008) *Die Auswirkung von duktilen Anschlüssen auf die Explosionsresistenz lasttragender Stützen* [Effect of Ductile Connections on Blast Resistant Load Bearing Columns]. *Stahlbau* 77(6): 436–446.

Starr CM and Krauthammer T (2005) Cladding-structure interaction under impact loads. *Journal of Structural Engineering: ASCE* 131(8): 1178–1185.

Su XY, Yu TX and Reid SR (1995). Inertia-sensitive impact energy-absorbing structures part I: effects of inertia and elasticity. *International Journal of Impact Engineering* 16(4): 651–672.

Vaughan DK (1983) *FLEX user's guide*. Report UG8298, May. Los Altos, CA: Weidlinger Associates, plus updates through 2015.

Vaziri A, Xue Z and Hutchinson JW (2006) Metal sandwich plates with polymer foam-filled cores. *Journal of Mechanics of Materials and Structures* 1(1): 95–125.

Vaziri A, Xue Z and Hutchinson JW (2007) Performance and failure of metal sandwich plates subjected to shock loading. *Journal of Mechanics of Materials* 2(10): 1947–1963.

Wardlaw AB, Luton JA, Renzi JR, et al. (2003) *GEMINI Euler solver for the coupled simulation of underwater explosions*. NSWCIHD/IHTR-2500. Indian Head Division Naval Warfare Center.

Winget DG, Marchand KA and Williamson EB (2005) Analysis and design of critical bridges subjected to blast loads. *Journal of Structural Engineering: ASCE* 131(8): 1243–1255.

Xue Z and Hutchinson JW (2003) Preliminary assessment of sandwich plates subject to blast loads. *International Journal of Mechanical Sciences* 45: 687–705.